Waste and Biomass Valorization
https://doi.org/10.1007/s12649-025-02930-z

ORIGINAL PAPER

Synthesis of Methyl Lactate from Glucose over Alkali-Modified Sn-H-Y Catalysts

Ramin Majidov[1] · Atte Aho[1] · Zuzana Vajglova[1] · Narendra Kumar[1] · Robert Lassfolk[1] · Ilari Angervo[2] · Teija Tirri[1] · Mika Lastusaari[3] · Kari Eränen[1] · Päivi Mäki-Arvela[1] · Jukka Hietala[4] · Dmitry Yu. Murzin[1]

Received: 30 May 2024 / Accepted: 19 January 2025

Abstract Glucose transformation to methyl lactate was investigated over microporous Sn-H-Y- zeolite with SiO_2/Al_2O_3 ratio of 30 as well as alkali metal modified mesoporous dealuminated Sn-H-Y-zeolites in the temperature range of 150-180°C. The catalysts were synthesized either by evaporation-impregnation or ion-exchange methods using a two-step procedure for Sn- and K-modification. The catalysts were characterized by several physico-chemical methods including SEM, TEM, pyridine adsorption-desorption FTIR, UV-VIS spectroscopy, solid state NMR-spectroscopy, nitrogen adsorption, TGA and CHNS for spent catalysts. The highest yield of methyl lactate of 72% was obtained at 150°C over dealuminated K-Sn-H-Y-30 catalyst at complete glucose conversion. Especially low K/Sn ratio was preferential for maximizing methyl lactate yield. Catalyst regeneration and leaching were also investigated.

Statement of Novelty The impact of potassium on mesoporous Sn-modified H-Y-30 was elucidated resulting in a very high yield of methyl lactate (72%) in glucose transformation over dealuminated K-Sn-H-Y-30 catalyst.

Keywords Glucose · Methyl lactate · Hierarchical zeolites · Tin

Introduction

The use of renewable feedstock for production of chemicals and fuels is currently under intensive research efforts. Especially the utilization of wood and agricultural waste should be promoted [1]. Due to the presence of a large amount of oxygen in the renewable feedstock in comparison to fossil feedstock, the main challenge is oxygen removal performed e.g. via hydrodeoxygenation of lignin derived feedstock or lipids to produce fuels [2]. Alternatively chemicals from biomass can be produced by acid hydrolysis of cellulose/hemicellulose [3] followed by their catalytic transformations [4, 5]. One potential product from hemicellulose/waste derived feedstock is lactic acid or its methyl ester, which can be made via fermentation [6] or catalytic transformation of sugars [4]. Methyl lactate can also be directly synthesized by one-pot transformation of cellulose [7]. Lactic acid finds application in cosmetics, pharmaceuticals, polymers, food and bevarages as well as in chemicals [8]. In addition methyl lactate and lactic acid can also be used as intermediates for production of acrylic acid via their dehydration [9]. A wide utilization of lactic acid is illustrated by its demand exceeding 1 Million tons in 2016 [10].

Glucose transformation has been intensively studied over Sn-modified Beta zeolites [11, 12], as well as alkali metal modified Sn Beta zeolites [13]. It has also been observed that mesoporosity or nanosized zeolites particles have positive effect on methyl lactate formation [14–19]. Especially high yields of methyl lactate were obtained over In-Sn-MCM-41 [19]. In addition to mesoporosity, also nanosized Sn-Beta catalysts with a high external surface have shown positive effects in glucose transformation to methyl lactate [20].

The use of an alternative approach, namely enzymatic catalysis, has a limited applicability resulting just in isomerization of glucose to fructose. This reaction is limited by thermodynamics, as the enzyme, glucose isomerase, has a

✉ Dmitry Yu. Murzin
dmurzin@abo.fi

[1] Johan Gadolin Process Chemistry Centre, Åbo Akademi University, Henriksgatan 2, Turku/Åbo 20500, Finland

[2] Wihuri Physical Laboratory, University of Turku, Turku 20014, Finland

[3] Department of Chemistry, University of Turku, Turku FI-20014, Finland

[4] Neste Corporation, Porvoo, Finland

Published online: 24 February 2025

limited thermal stability and cannot be used at temperatures (ca. 150°C) required for splitting the carbon-carbon bonds. Another alternative is to apply homogeneous catalysis with an obvious obstacle related to challenges in catalyst separation and recovery from the products.

Glucose transformation to methyl lactate is a very complicated reaction (Scheme 1). The desired reaction starts with glucose isomerisation to fructose, a desired ketohexose, which thereafter should undergo [3+3] retro aldol cleavage forming pyruvic aldehyde, which in turn reacts via H-shift and methanol addition to methyl lactate. There are, however, also several side reactions such as glucose epimerization to mannose and [2+4] retro aldol of both aldohexoses glucose and mannose, forming vinyl glyoxal through H-shift and methanol addition giving methyl vinyl glycolate [21]. In addition, glucose can react with methanol in a reversible way forming an ether, a-methylglucopyranoside [13]. Alternatively, fructose can dehydrate over strong Brønsted acid catalysts to 5-hydroxymethylfurfural, which in turn can be etherified to 5-methoxymethylfurfural. 5-hydroxymethyl furfural in the reaction with methanol gives both methyl levulinate and methyl formate [4]. In addition, humin formation is also well-known in sugar transformations [7]. Moreover, sugar oligomers can be formed, which are not visible in typical gas or liquid chromatographic analysis.

The aim of this work was to compare the performance of microporous Sn-modified H-Y zeolite with the SiO_2/Al_2O_3 ratio of 30 and dealuminated Sn- and/or alkali metal modified H-Y zeolite with the same SiO_2/Al_2O_3 ratio in glucose transformation to methyl lactate. According to our knowledge H-Y zeolites have not been used as supports in glucose transformations. In addition to support acidity, also the effect of alkali modification, i.e. Sr, K, or Cs, was investigated on Sn-modified H-Y-zeolite. The main aim was to optimize the catalyst properties and maximize the methyl lactate yield. Several different characterization methods were applied, such as nitrogen adsorption-desorption, transmission emission and scanning electron microscopy, energy dispersive X-ray analysis, X-ray diffraction, UV-VIS spectroscopy, solid state NMR-spectroscopy, pyridine adsorption desorption with FTIR, temperature programmed desorption of CO_2, CHNS-analysis and inductively coupled plasma spectroscopy to correlate catalyst properties with their performance.

Materials and Methods

Materials

The chemicals, applied in this work were used without any purifications (see Table S1). As a comparison some preliminary experiments were also performed with commercial H-Y-5.1 and H-Y-80 zeolites as reported in [22].

Methods

Catalyst Synthesis

Evaporation impregnation (EIM) method was applied for synthesizing several Sn modified zeolite catalysts. Both tin (II) and tin (IV) chlorides were used as precursors applying the following method: 3.5 g of the precursor was dissolved

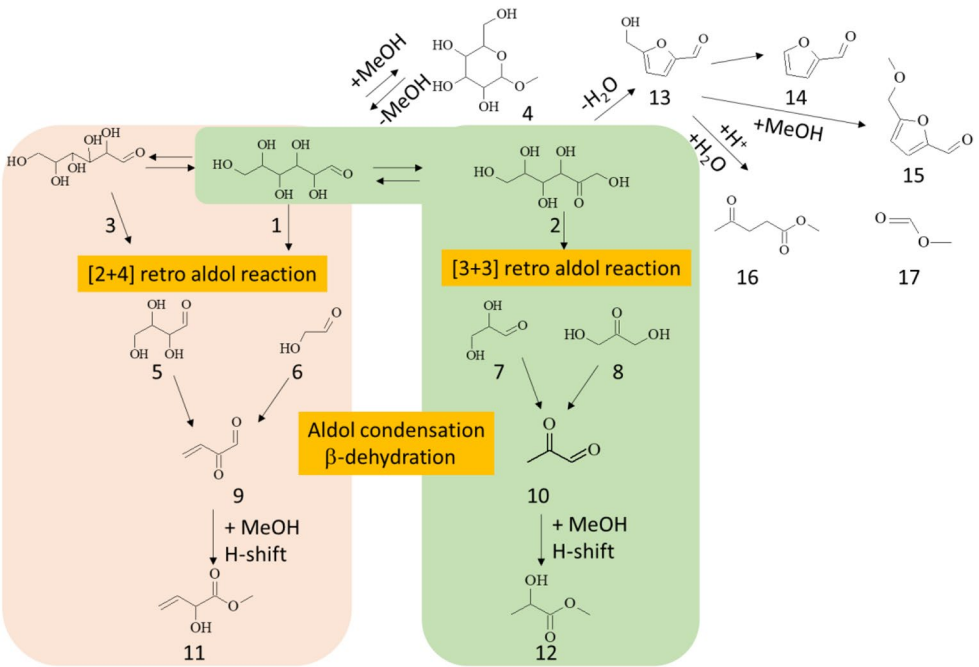

Scheme 1 Reaction network for glucose transformation at 150-180°C in methanol over an acidic catalyst. Notation: 1. Glucose (GLU), 2, fructose (FRU), 3 mannose (MAN), 4, a-methyl-glucopyranoside (GLUPYR), 5. tetrose saccharides, 6. glycolaldehyde, 7. glyceraldehyde, 8. dihydroxyacetone, 9. vinylglyoxal, 10. pyruvic aldehyde, 11. methyl vinyl glycolate (MVG), 12. methyl lactate (MeLa), 13. 5-hydroxymethyl furfural (HMF), 14. Furfural (FU), 15. methoxy methylfurfural (MMF), 16. methyl levulinate (MeLe) and 17. methyl formate (MeFo)

in 250 ml of water (pH range of the obtained solution was ca. 1.5–1.8) followed by addition of 10 g of the zeolite. Thereafter pH was in the range of ca. 1.7–2.0. Finally, the catalysts were synthesized in a rotavapor for 24 h at 50 °C and 60 rpm and the solvent was removed after synthesis by evaporation. The following step-calcination process was used to calcine the catalyst after drying at 100 °C in an oven for an entire night: 250ºC (40 min)- 2.5 ºC/min- 550 ºC-240ºC and cooled down to room temperature. The applied heat treatment protocol follows the step calcination procedure for decomposition of the tin precursor applied previously for preparation of Sn containing zeolites ensuring good dispersion of Sn metal nanoparticles [13].

Dealumination of H-Y was performed by treating the material with 10 M 70% aqueous nitric acid solution for 1 h following the procedure of [17]. Thereafter, the slurry was filtered and neutralized with distilled water until pH close to 7 was reached. The washing procedure was repeated two times followed by filtration. Thereafter, the filtered catalyst was dried overnight at 100 °C. These steps were repeated 2–4 times which is reflected in the notation for dealuminated H-Y-30 catalysts, namely for H-Y-30-DA-x materials, x indicates how many times the dealumination of the support was performed. Tin modification was done by adding into an aqueous $SnCl_4$ solution the dealuminated support followed by stirring for 5 h, drying at 100ºC overnight and calcination at 550ºC. Triethylamine was used as an activator in metal grafting facilitating creation of Sn-O-Si bonds [17]. In the second step, K modification was performed in the following way: 250 ml of 0.5 M aqueous solution of KCl was combined with the Sn-modified catalyst and the mixture was stirred for 2 h at room temperature. The final catalyst was filtered, dried at 110 °C overnight, and calcined at 550 °C for 6 h with the same step calcination procedure as given above. H-Y supports with three different SiO_2/Al_2O_3 ratios were modified with Sn and K. In the catalyst notation, Sn indicates $SnCl_2$, while DA and EIM reflect respectively dealumination and EIM evaporation impregnation method. In addition, the number before Sn indicates its content in wt% determined by ICP, if not stated otherwise.

Strontium and cesium were loaded in Sn-modified H-Y zeolites by the incipient wetness method using either 0.5 M solutions of $Sr(NO_3)_2$ or $CsNO_3$ precursors, which were slowly added to the Sn modified H-Y zeolites with the SiO_2/Al_2O_3 ratio of 30 under 100 rpm stirring. Thereafter, the mixture was stirred for 2 h followed by filtration. Finally, the catalyst was washed twice with deionized water, dried at 100 °C and calcined at 550 °C for 6 h.

The spent catalysts from the reaction were regenerated with the step-calcination procedure. The following method was used to regenerate the spent catalyst: 225 ºC (75 min)-3ºC/min-400ºC (120 min). The regenerated catalyst was then evaluated for its catalytic performance in the subsequent reaction cycle.

Catalyst Characterization

The phase purity and crystal phases in different catalysts were investigated with powder X-ray diffraction (XRD using the Bragg-Brentano configuration and the CuKα radiation and a one-dimensional LynxEye detector. The angular range from 15° to 70° with a step of 0.05° and the acquisition time of 3 s at each point were applied. From the broadening of the diffraction peaks, the sizes of the coherently scattering domains (CSD – D_{XRD}) were calculated. As a standard α-Al_2O_3 (SRM 1976) [23] was used, and the instrumental broadening of the diffraction lines was taken into consideration.

A PANalytical Empyrean diffractometer with a five-axis goniometer was used for XRD-measurements. The incident beam optics included a Bragg-Brentano HD X-ray mirror, a fixed 1/4º divergence slit, a 10 mm mask, a 0.04 rad Soller slit, and a 1° anti-scatter slit. The optics for the diffracted beam included a PIXcel detector array, a 0.04 rad Soller slit, and a 7.5 mm divergence slit. The used X-ray equipment was an Empyrean Cu LFF tube. Only the Cu Kα1 and Cu Kα2 components of the X-ray radiation were kept out by a filter.

The Jeol JEM-1400Plus instrument with a 120 kV acceleration voltage and a resolution of 0.38 nm, was used to study the metal particle size, textural characteristics, porosity, and periodicity of pores of the catalysts. Before the TEM measurements, the majority of the Sn-based catalysts were calcined.

The crystal morphology of the prepared catalysts was investigated using SEM, and EDX was used to ascertain their elemental compositions. SEM measurements were carried out using a Zeiss Leo Gemini 1530 Scanning Electron Microscope and a Thermo Scientific UltraDry Silicon Drift Detector (SDD). The X-ray analyzer was operated at an acceleration voltage of 15 kV.

The Micromeritics 3Flex-3500 instrument was used for the surface area measurements. For ex-situ treatment of samples ca. 50–100 mg of the catalyst was heated overnight at 180 °C under vacuum of 0.2–0.3 bar. The adsorption isotherms were measured at -196 °C. The Dubinin-Radushkevich method was used to determine the specific surface areas of the synthesized microporous materials. The DFT method was used to determine the pore size distribution of the catalysts.

ATI Mattson FTIR was used to perform the qualitative and quantitative analysis of the catalyst Brønsted and Lewis

acid sites with pyridine as a probe molecule. The catalyst was prepared as a thin, self-supporting pellet with the mass of 15–30 mg and radius of 0.65 cm, which was then placed inside the FTIR cell. For pretreatment, the cell temperature was raised to 450 °C under vacuum and maintained for an hour. Thereafter, a background spectrum of the sample was captured while the temperature was lowered to 100 °C. The probe molecule (pyridine) was adsorbed at 100 °C for 30 min and then desorbed by evacuation at various temperatures. The three desorption temperatures were 250 °C for weak, medium, and strong acid sites, 350 °C for medium and strong, and 450 °C for strong acid sites. At each step of the temperature ramp, the spectra of the adsorbed pyridine were recorded. Spectral bands at 1545 cm^{-1} and 1450 cm^{-1} were used, respectively, to distinguish between Brønsted and Lewis acid sites, respectively during scanning, which was carried out in vacuum of 10^{-2}-10^{-1} bar at 100 °C. Using the molar extinction parameters published in ref [24]. the acid sites were quantified.

UV-vis DRS analysis was performed for some catalysts to distinguish the Sn species and to compare the data with the catalyst performance. The measurements were performed with an Avantes Avaspec HS-TEC CCD spectrometer connected to an Avantes FC-UV600-1-SR fiber optic cable using an Avantes AvaLight-DHc light source with halogen and deuterium lamps. The white reference was a $BaSO_4$ disc (Edinburgh Instruments).

The ^{29}Si and ^{27}Al MAS NMR spectra were recorded on a Bruker AVANCE-III spectrometer operating at 79.50 MHz (^{29}Si) and 104.26 MHz (^{27}Al) and using a CP-MAS 4 mm solid state probe. The following parameters were used to record the ^{27}Al spectra: a 5.00 µs pulse and a recycle delay of 0.05 s at 14 kHz spinning speed. The ^{29}Si spectra were recorded using a 3.84 µs pulse and a recycle delay of 100 s at 14 kHz spinning speed.

The possible metal leaching from the catalyst into the liquid phase was investigated by analyzing the filtrated liquid phase sample after 24 h of the reaction with Inductively Coupled Plasma (ICP). Methanol was removed from the product mixture by purging it with nitrogen. Thereafter, 3.6 ml of hydrochloric acid (65%, Sigma Aldrich) and 1.2 ml of nitric acid (70%, Sigma Aldrich) were added to the product to achieve an optimal concentration for the equipment. The resulting solution was transferred into a 100 ml volumetric flask, ensuring that the walls of the beaker were thoroughly rinsed with an in-situ prepared aqua regia and the solution was then diluted with distilled water to a final volume of 100 ml. Once the sample was prepared and measured, the discrepancies in metal concentrations between the two different media could be detected.

The filtration test was performed for the reaction mixture after removal of the catalyst from it. The reaction which was carried out with 2 wt% Sr – 2 wt% Sn/H-Y-30-DA catalyst for 24 h, was stopped for cooling and separation of the reaction mixture from the solid catalyst. The catalyst was filtered using the filter paper (Whatman, 2 µm pore size) with a further filtration using PVDF syringe filter, (0.45 µ). The filtrate was loaded into the autoclave, heated to 150 °C and run for another 24 h.

Catalyst Testing

Experiments were carried out in a batch mode using an autoclave using 0.75 g of the catalyst, if not otherwise stated, and 0.066 mol/l glucose in 75 ml of methanol. After loading the reactor, it was flushed with argon 3–5 times. Thereafter, the heating of the reactor was started at a 3 °C/min heating rate. When the desired reactor temperature was reached, the total pressure was adjusted to 30 bar and the reaction was started when the stirring was put on. A high stirring speed (720 rpm) and small catalyst particles (< 64 µm) were used to suppress the internal and external mass transfer limitations. The samples were taken from the reactor at different reaction times.

Analysis of Products

The liquid samples were analyzed both with HPLC and GC techniques. The following HPLC method was used: Hewlett Packard 1100 series instrument equipped with a refractive index detector (RI), while the column used for separation of the compounds was an Animex HPX-87 H applying 5 mM sulphuric acid as the eluent at °C and using 0.6 ml/min flow of H_2SO_4. Response factors as well as the retention times for several different compounds were determined before catalytic experiments and used for calculations of the concentrations.

The sample was further analyzed by gas chromatography to quantify methyl lactate, methyl levulinate, as well as furfural and methyl formate after achieving in practice full conversion of glucose. The GC was an HP 6890 Series GC System with an HP-5, 5% phenyl methyl siloxane column of 30 m length, internal diameter 320 µm and the film thickness 0.50 µm and a flame ionization detector (FID). The analysis used the following temperature program: 2 min at 40 °C, 10 °C/min heating to 250 °C, holding for 3 min, and 3.8 ml/min of the gas flow rate through the column. Different components were calibrated for GC analysis and the retention times are shown in Supporting information in Table S2. The unknown compounds in the product samples were identified using gas chromatography and mass spectrometry.

CHNS analysis was carried out using a Thermo Fischer Scientific Flash organic elemental analyzer equipped with

TC detector. The measurement was performed at 950°C and the elements were quantified using cystine, 2,5-bis(5-tert-butyl-benzozazol-2-yl)thiophene, methionine and sulphanilamide as standards.

Thermogravimetric analysis was performed with SDT650 instrument to detect adsorbed organic residue on the spent catalyst surface. The following temperature programme was applied: 10 °C/min −800°C (1 min) and the measurements were performed under air atmosphere.

Formulae and Definitions

Conversion of glucose (X) was calculated by:

$$\mathrm{X}\,(\%) = 100^{*}\frac{\mathrm{n_{GLU,0}} - \mathrm{n_{GLU,\,F}}}{\mathrm{n_{GLU,0}}} \tag{1}$$

Where, $\mathrm{n_{GLU,0}}$ and $\mathrm{n_{GLU,\,F}}$ are the initial and final moles of glucose, respectively. The liquid phase mass balance of compounds (MB) was calculated by:

$$\mathrm{MB}\ (\%) = 100^{*}\ \frac{\mathrm{MB_f}}{\mathrm{MB_0}} \tag{2}$$

Where $\mathrm{MB_f}$ is the sum of liquid-phase reactants and products at the end of the reaction (time 24 h), and $\mathrm{MB_0}$ is the sum of liquid-phase reactants at the beginning of the reaction (time 0).

The yield of methyl lactate was calculated by:

$$\mathrm{Y}\,(\%) = 100^{*}\frac{(\mathrm{n_{MeLa,1400}})\,/2}{\mathrm{n_{GLU,0}}} \tag{3}$$

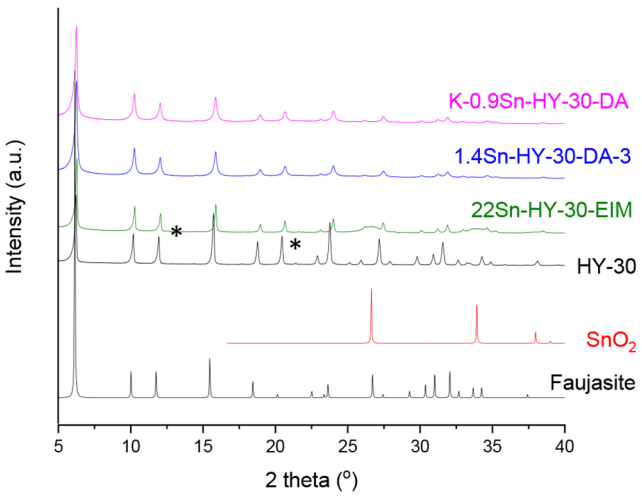

Fig. 1 XRD results of the catalysts. Notation: SnO_2 *

Where $\mathrm{n_{MeLa,1400}}$ is the final molar amount of methyl lactate. Notation $\mathrm{n_{MeLa,1400}}$ is the moles of methyl lactate after 1400 min reaction time.

Selectivity was calculated by this equation:

$$\mathrm{S}\,(\%) = 100^{*}\mathrm{Y}/\mathrm{X_{GLU}} \tag{4}$$

Where S denotes selectivity, Y yield and $\mathrm{X_{GLU}}$ glucose conversion. Carbon balance (CB) in the liquid phase products was calculated as:

$$CB = \frac{\sum n_{i,j}.CN_i}{n_{GLU,0}.CN_{GLU}} \tag{5}$$

where *CB* denotes carbon number in molecule i, n_i mole of component *i* and $n_{GLU,0}$ the initial glucose amount in moles.

Results and Discussion

Catalyst Characterization Results

X-ray Diffraction

X-ray diffraction measurements were performed for four different catalysts (Fig. 1). The results showed that XRD patterns for different catalysts matched well with standard structures of both faujasite zeolite [25, 26] and SnO_2 [27]. For faujasite the reference ICSD 41,398 corresponds to the zeolite phase with cubic symmetry (space group Fd-3 m) and cell parameter of 24.630 Å.

Especially, the diffraction pattern of Sn-H-Y-30-EIM revealed clear details confirming the presence of SnO_2 phase [26] with the volume percentage of 3%. Due to the low signal intensity for SnO_2 phase in Sn-H-Y-30-DA and K-0.9Sn-H-Y-30-DA, its identification is not considered reliable.

Scanning Electron Microscopy and Energy Dispersive X-rays Analyses (SEM-EDX) and ICP-OES Analyses

The scanning electron microscopy (SEM) images of microporous Sn-H-Y-30-EIM are shown in Fig. 2. For this catalyst, the crystal sizes varied in the range of 210–520 nm and several shapes were observed, such as pyramidical, hexagonal, triangular or rectangular ones.

It can be speculated that the reasons for the different morphologies such as pyramidical hexagonal, triangular or rectangular of the synthesized catalysts can be attributed to the methods of the catalyst preparation such as evaporation impregnation and also dealumination, influencing the crystal structure.

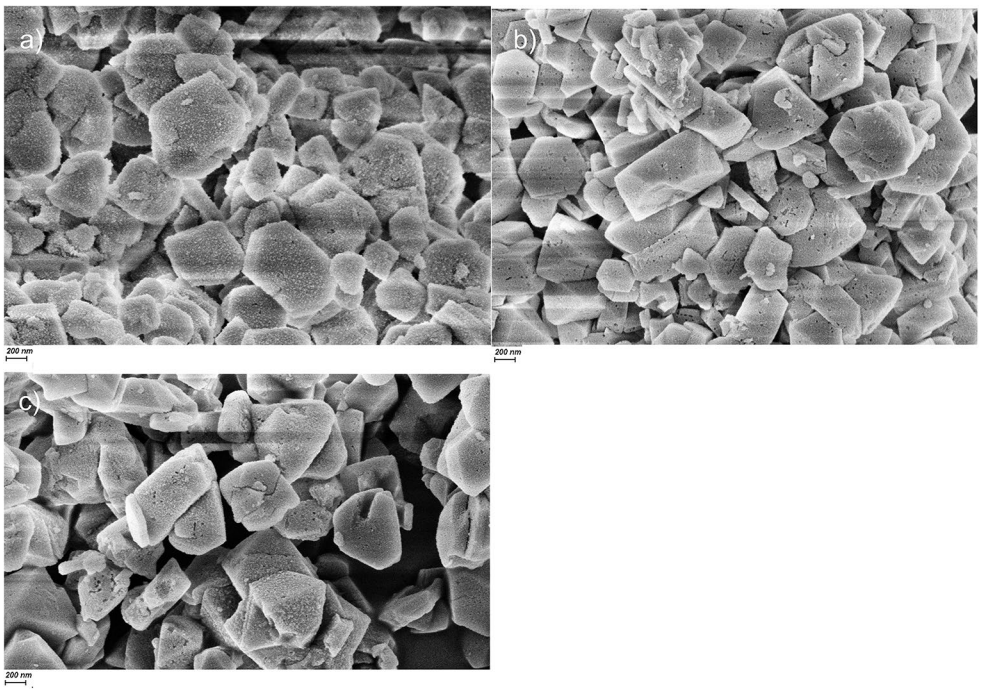

Fig. 2 SEM images of (**a**) 22Sn-H-Y-30-EIM, (**b**) 1.4Sn-H-Y-30-DA and (**c**) K-0.9Sn-H-Y-30-DA. Notation: scale bar in all Fig. 200 nm

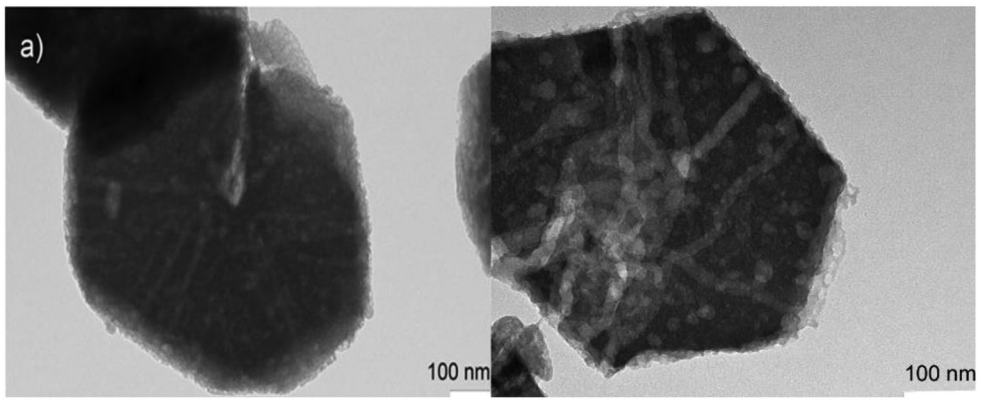

Fig. 3 TEM images of (**a**) H-Y-30 and (**b**) H-Y-30-DA

Uniform distribution of tin is also clearly visible. It was earlier reported that $SnCl_2$ modification of H-Y resulted in formation of small Sn particles and small crystal, because $SnCl_2$ exhibits high reactivity [28].

SEM images of dealuminated Sn-H-Y-30-DA depicted in Figs. 2 and 3 demonstrate that creation of mesopores when using 10 M nitric acid. During dealumination large particles can break down and open new channels [29]. Furthermore, other textural properties, such as the surface area and the pore size distribution have changed (see Table 1). Despite of the nitric acid treatment, the crystallites are well-structured and vary in the size between 220 and 900 nm. K-modification did not change crystal shapes or sizes. Cavities are more clearly visible in TEM images (see below).

The elemental analysis results of different catalysts showed that aluminium content in the dealuminated catalysts is low as expected (Table 2). The metal content was analyzed by ICP-MS for different fresh dealuminated K-Sn-H-Y-DA catalysts. Sn content was varied in the range of 0.87–3.61 wt%, while amounts of potassium were rather low.

More accurate determination of elements was obtained by ICP measurements, which were used to correlate catalytic data. In addition, the ICP-MS analysis of the possible metal leaching from the spent K-0.9Sn/H-Y-30-DA used in glucose transformation at 150°C for 24 h showed that the total amount of leached metals was found to be 15.5 wt% and 6.4 wt% for Sn and K, respectively. This result is in line with those reported in [17], in which 80% loss of potassium content was observed in the spent catalyst used in glucose transformation.

Transmission Electron Microscopy (TEM)

TEM images of some selected catalysts are shown in Figs. 4–5 while the average particle sizes of Sn are given

Table 1 Textural properties of the fresh and spent catalysts. Notation: in parenthesis the data for spent catalysts are given. Surface area given as BET for mesoporous and the Dubinin method for microporous catalysts. All sn catalysts reported in this table were prepared from SnC_2

Entry	Catalyst	Surface Area (m^2/g)		D av. (nm)	Total Pore Volume (cm^3/g)	Total Pore Volume (cm^3/g) t-plot	Vmicro (%)	Vmeso (%)	Vmicro/Vmeso
		BET	Dubinin						
1.	H-Y-30	816	1217	0.66, 0.77	0.42	n.a.	68	32	2.1
2.	H-Y-30-DA-3	502	653	0.66, 0.77	0.33	n.a.	70	30	3.2
3.	22Sn-H-Y-30-EIM[a]	376	526 (440)	0.77	0.25 (0.24)	0.13	75 (65)	25 (35)	3.0 (1.9)
4.	0.9Sn-H-Y-30-DA	753	712	0.84	0.33	0.16	76	24	3.2
5.	1.4Sn-H-Y-30-DA	435	590	0.84	0.27	0.15	77	23	3.3
6.	K-1.4Sn-H-Y-30-DA		547	0.84	0.33	n.a.	61	39	1.6
7.	K-0.9Sn-H-Y-30-DA	437	525 (514)	0.84	0.30 (0.30)	0.10	61 (55)	39 (44)	1.6 (1.3)
8.	K-3.6Sn-H-Y-30-DA-2	437	738	0.84	0.33	0.19	78	22	3.5
9.	K-1.3Sn-H-Y-30-DA-4		642	0.84	0.33	n.a	72	28	2.6
10.	Cs-0.6Sn-H-Y-30-DA[a]	n.d.	760	0.84	0.37	n.a.	73	27	2.7
11.	Sr-2.5Sn-H-Y-30-DA[a]	n.d.	720	0.84	0.35	n.a	74	27	2.7

[a]nominal Sn content in the name

Table 2 SEM-EDX analysis of the fresh and spent catalysts. In parenthesis the wt% of elements are given for the spent catalysts. Notation: n.d. not determined, n.a. not available. No cl was observed in any sample

Entry	Catalyst	O	Al	Si	K	M[a]	Sn	Al/Si	Al/Sn
1	22Sn-H-Y-30-EIM[a]	46 (65)	3 (2)	35 (36)	0	0	16 (10)	0.09 (0.05)	0.2 (0.2)
2	Sr-2.5Sn-H-Y-30-DA	69	0.74	26.4	0	1.9	1.9, 2.5 [b]	0.03	0.30
3	Cs-0.6Sn-H-Y-30-DA	70	0.9	26	0	1.0	2.4, 0.6[b]	0.03	0.38
4	1.4Sn-H-Y-30-DA	52	1.57	45	0	0	1.4	0.03	1.12
5	K-0.9Sn-H-Y-30-DA	53 (71)	1 (0.9), 0.45[c]	45 (28)	0, 0.11[c]	0	1.3 (0), 0.87[c]	0.02 (0.03)	0.78 (very large)
6	K-1.3Sn-H-Y-30-DA-4	70	0.72	27	0.13, 0,29[c]	0	1.4, 1.32[c]	0.03	0.50
7	K-1.4Sn-H-Y-30-DA-3	52	0.43	45	0.15[c]	0	1.7, 1.43[c]	0.1	0.27
8	K-3.6Sn-H-Y-30-DA-2	52	0.46	45	0.21[c]	0	2.3, 3.61[c]	0.01	0.13

[a] nominal loading of Sn, [b]Sr or Cs, [c] ICP analysis.

in Table 1. The TEM image of the commercial parent H-Y-30 shows that there are also some large cracks, which have formed when the material was steamed and acid leached during its manufacturing process [30, 31].When comparing the structure of the parent H-Y-30 zeolite with its dealuminated counterpart (Fig. 3) it can be clearly seen that more large cavities are formed during dealumination and that the catalyst morphology changed using 10 M nitric acid for dealumination. The images of dealuminated Y zeolites demonstrate a decrease in the catalyst particle size (Fig. S1b), for example from 1035 nm (Fig. S1a) to 970 nm (Fig. S1b). The images also illustrate the presence of new defects in the zeolite structure as also visible in nitric acid treated dealuminated USY zeolite [29].

It should, however, be noted that relatively large Sn particle sizes of Sn for microporous support also are due to a large loading of tin. For mesoporous delaminated catalysts the average particle size of Sn also increased with increased tin loading. Agglomeration of $SnCl_2$ modified H-Y-30-DA-4 catalyst particles is also visible in Fig. S1c. Overall the average Sn particle size was smaller for K-Sn-H-Y-30-DA than for the microporous Sn-modified catalysts (Fig. 4, Fig. S1). In addition, the Sn particle size increased as follows for different alkali metal modified Sn-H-Y-30-DA-2 catalysts: K < Cs < Sr, which is the order of increasing Sn content (Table 2).

The TEM images of parent and K-Sn-modified H-Y-30-DA reveal aggregation of the metal nanoparticles and the extent to which they are located on the external surface of the catalyst particle. It is however, difficult to separate Sn and K particles due to their closer particle sizes. Large cavities are clearly visible in dealuminated zeolite (Fig. 5a) as in [14]. It can, however, be stated that the pores and channels of Y zeolite were intact even after synthesis and modifications with Sn and K. Based on TEM images it is difficult to assess if the placement of metal particles in the catalyst channels has been successful.

Comparing fresh and spent K-0.9Sn-H-Y-30-DA catalysts (Fig. 5) it can be seen that the fresh H-Y-DA catalysts typically exhibit well-defined crystalline structures with regular pore arrangements, while in the spent catalysts, structural changes like framework collapse, dealumination,

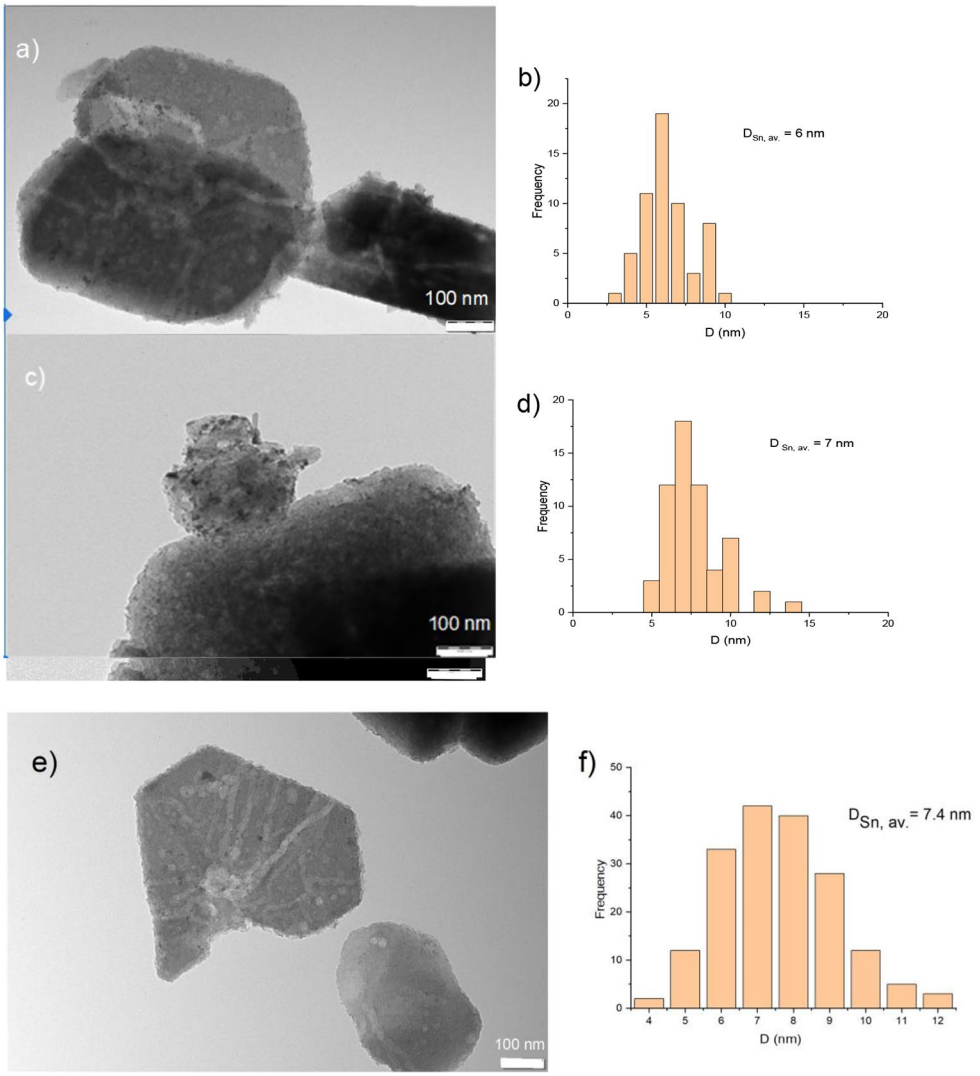

Fig. 4 **a**, **c**, **e**) TEM images and **b**, **d**, **h**) the corresponding Sn particle size distribution and TEM images Cs-, Sr- K-modified Sn-H-Y-30-DA-2, **e**, **f**) the corresponding pictures for K3.6Sn-H-Y-30-DA-2

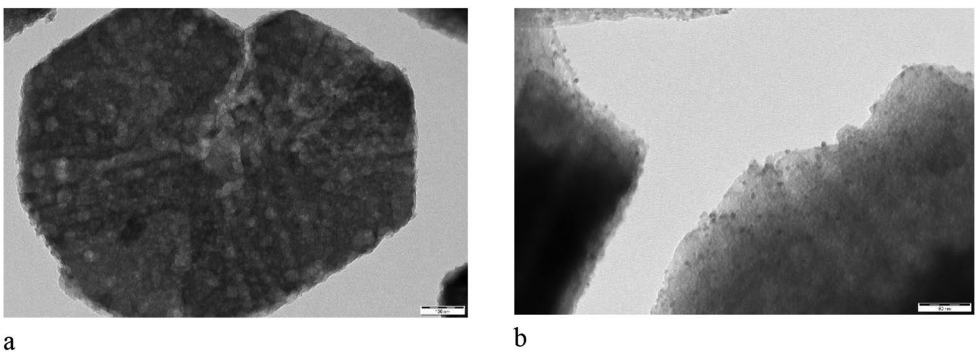

Fig. 5 TEM images of **a**) H-Y-30-DA, scale bar is 100 µm and Sn-H-Y-30-DA, scale bar 50 µm

metal leaching, or the formation of secondary phases may be observed, leading to alterations in the particle morphology and the size. Some sintering and uneven distribution with a less uniform morphology can be seen in K-0.9Sn-H-Y-30-DA catalyst (Fig. 5b). The average particle sizes of the spent Sn, K, and K-Sn catalysts synthesized with the dealuminated H-Y-30 supports were slightly larger (2–5%) than for the fresh catalysts. This confirms that there was sintering of Sn and K nanoparticles during the reaction as observed in lactic acid formation from glycerol [32].

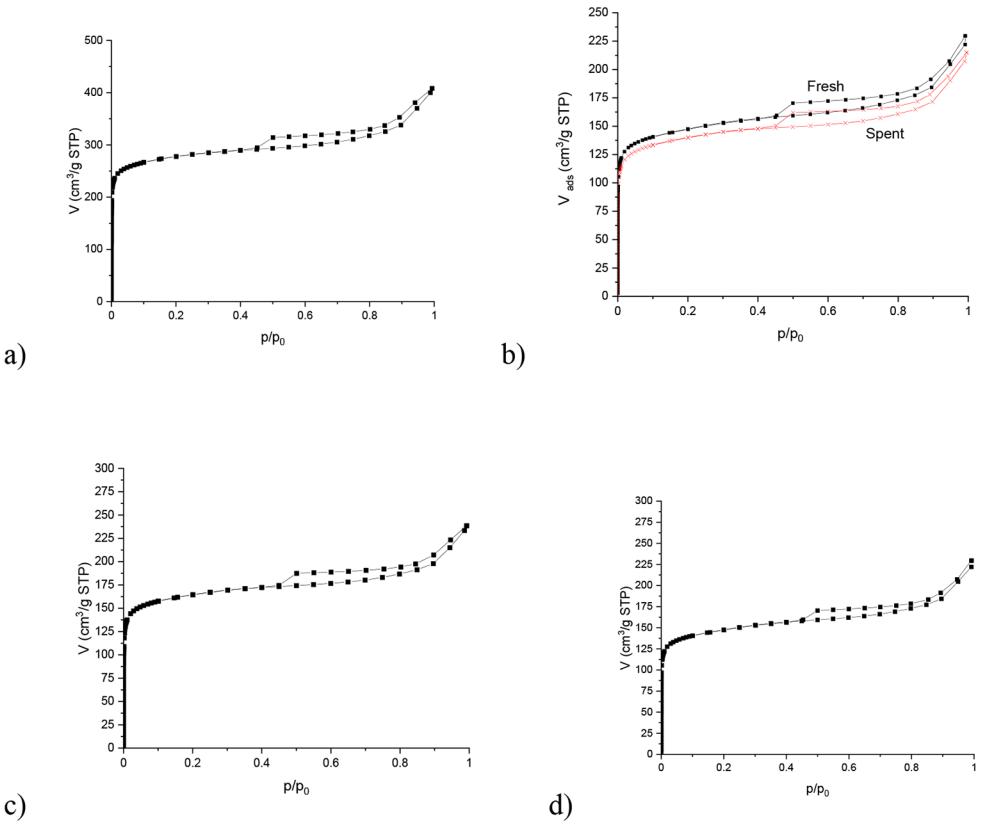

Fig. 6 The nitrogen adsorption-desorption isotherms for (**a**) fresh H-Y-30, (**b**) fresh and spent K-0.9Sn-H-Y-30-DA, **b**) fresh K-3.6Sn-H-Y-30-DA-2, (**c**) fresh K-1.3Sn-H-Y-30-DA-4

Nitrogen Physisorption

>Textural properties of the catalysts are shown in Table 1. Surface areas of the catalysts were calculated by both BET and Dubinin methods, because the latter one is especially developed for microporous materials, while for BET the multilayer adsorption is assumed, clearly contradicting with the size of micropores. The surface area calculated by the Dubinin-Radushkevich surface areas for H-Y zeolites which were synthesized by evaporation impregnation method, while for mesoporous catalysts the BET method was used. The results show that the ratio between micro- to mesopore volumes for the parent zeolites, Sn modified zeolites and dealuminated zeolites decreased when increasing the SiO_2/Al_2O_3 ratio. The results also indicated that incorporation of Sn into the H-Y zeolite led to a decrease in the surface area compared to the pristine zeolite. A typical adsorption-desorption isotherms of the parent H-Y-30 and dealuminated K-Sn-H-Y-30 with different Sn loading are clearly showing the hysteresis starting at p/p_0 of 0.45 behaviour (Fig. 6) analogously to [17].

The pore size distribution in the microporous range is depicted both for microporous H-Y-30 as well as dealuminated and also Sn- and K-modified dealuminated counterparts (Fig. 7). The parent H-Y-30 contained also mesopores as also noted in [32]. This picture shows that dealumination

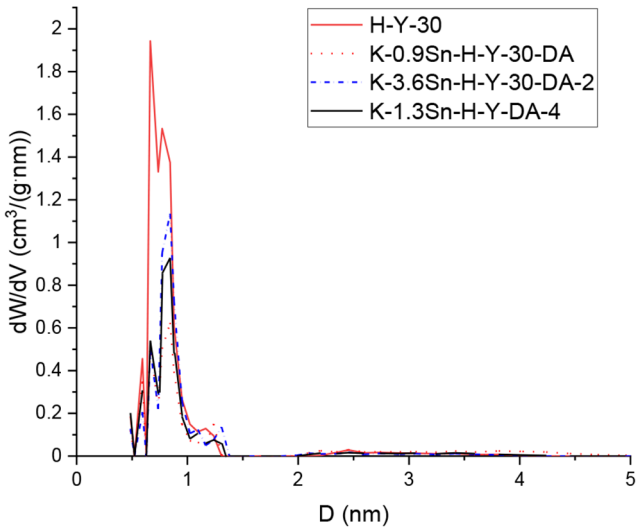

Fig. 7 Pore size distribution for some fresh catalysts

and even more modification of both potassium and tin diminishes the micropore volume in most cases, except for K-3.6Sn-H-Y-30-DA-2. Especially the ratio between the micro pore volume to mesopore volume was low for K-0.9Sn-H-Y-30-DA and K-3.6Sn-H-Y-30-DA-4 (Table 1).

The nitrogen physisorption results of the fresh and spent H-Y zeolites are shown in Table 1. As expected, the Dubinin method gave a higher surface area compared to the BET

method. Furthermore, notable differences in the pore structure and surface properties of the zeolites after their exposure to specific conditions were observed (Table 1). For the more acidic 22Sn-H-Y-30-EIM catalyst, the specific surface area of the spent catalyst decreased 16% in comparison to the fresh one (Table 1, entry 3). This indicates accumulation of organic compounds on the surface of the catalyst. An analogous decrease in the surface area after glucose transformation was observed for the spent [K]Sn-USY in [16].

Surface area changes between the fresh and spent catalysts were also observed for other dealuminated and metal-modified H-Y zeolites displaying minor decrease in surface areas within the range of 88–95%. The decline in the surface area of the spent catalysts can be attributed to accumulation of the reaction by-products and pore blockage as reported in [17].

As follows from the nitrogen physisorption data, namely hysteresis for the desorption branch, the materials applied in the present study contain mesoporosity. Such mesoporosity is essential in enhancing the mass transfer through the transport pores. The impact of the textural properties (micro/meso pore volume) on catalytic behavior including selectivity is less apparent as tin oxide is present outside of the pores.

Catalyst Acidity and Basicity

Acidity of the catalysts determined by pyridine adsorption-desorption- FTIR show that Brønsted acidity decreased for the dealuminated H-Y-30-DA-4 in comparison to the parent H-Y-30. The microporous 22Sn-H-Y-30-EIM exhibited also 60% of the Brønsted acid sites in the parent H-Y-30. The BA/LA ratio was the highest (Fig. S2), as expected for H-Y-30, while this ratio was also unexpectedly high for K-0.9Sn-H-Y-30-DA (Table 3, Fig. S2). Among K-, Cs- and Sr-modified catalysts the highest BA/LA acid ratio was observed for K-Sn-H-Y-30-DA, while a very low BA/LA ratio was determined for Sr-Sn-H-Y-30. Noteworthy is that K-Sn-H-Y-30-DA exhibits only Lewis acidity. These results are in accordance with [33] reporting that dealumination decreased Brønsted acidity as well as strong Lewis acid sites.

A comparative study for some selected catalysts was performed using both ^{27}Al solid state NMR-spectroscopy and UV-VIS method. The UV-vis results revealed large variations in the dealumination step during synthesis of these catalysts (Fig. 8a). The absorption peak close to 200 nm is originated form framework Sn^{4+} and it has been reported to have high intensity with high Sn loadings [34, 35], as is the case in the current work. In H-Y-30-DA spectrum a peak at 280 nm exhibits high intensity and is related to the presence of extra framework Al species [36]. The bands at higher region, i.e. 245 nm and 275 nm, which are clearly visible for all Sn-modified catalysts in Fig. **8**a, are related to extraframework SnOx species and bulk SnO_2 [34].

The results from solid-state NMR-spectroscopy are well in line with the results from the UV-vis study (Fig. 8b). The band at 60 ppm signal originates from the four-coordinated framework Al i.e. Brønsted acid sites, while the peak at ca. 30 ppm arises from the five-coordinated extra-framework Al, and the resonance at 0 ppm corresponding to Lewis acid sites is associated with six-coordinated extra-framework aluminium [37, 38]. The amount of Brønsted acid sites declined after inclusion of potassium and Sn, and the latter one is a Lewis acid itself, subsequently the amount of Lewis acid sites is increasing and the introduction of K results in an decrease of the overall Brønsted acidity in the framework species. The highest amount of framework tetrahedral aluminium species were found in 1.4Sn-H-Y_30-DA followed by H-Y-30-DA. It should, however, be stated that based on pyridine adsorption-desorption, some weak and medium Brønsted acid sites are still present (Table 3) due to incomplete removal of aluminium during dealumination (Table 2). The smallest peak area for tetrahedral aluminium species was observed for K-3.6-Sn H-Y-30-DA-2. The Brønsted acidity is originated from the remaining aluminium and the

Table 3 The amounts of Brønsted and Lewis acid sites for pristine proton forms and Sn-modified catalysts determined by FTIR pyridine adsorption-desorption. Notation: weak acid site, medium acid site and strong acid site, BA Brønsted acid site and LA Lewis acid site

	Catalyst	Brønsted acidity (μmol/g)			Total BA (μmol/g)	Lewis acidity (μmol/g)			Total LA (μmol/g)	BA/LA
Entry		Weak	Medium	strong		Weak	Medium	strong		
1	H-Y-30	38	108	13	159	4	8	1	13	11.2
2	H-Y-30-DA-4	7	34	26	67	9	0	5	14	4.8
	K-H-Y-30-DA	0	0	0	0	48	0	0	48	0
3	22Sn-H-Y-30-EIM	4	8	76	88	1	4	15	20	4.5
4	K-0.9Sn-H-Y-30-DA	28	13	0	41	0	5	0	5	8.2
5	K-1.3Sn-H-Y-30-DA-4	17	0	0	17	4	0	0	4	4.3
6	K-1.4Sn-H-Y-30-DA-3	4	17	0	21	1	5	0	6	3.5
7	K-3.6Sn-H-Y-30-DA-2	4	16	0	20	21	6	0	27	0.74
8	Cs-0.6Sn-H-Y-30-DA	11	0	0	11	7	0	0	7	1.6
9	Sr-2.5Sn-H-Y-30-DA	2	1	12	15	20	1	4	25	0.6

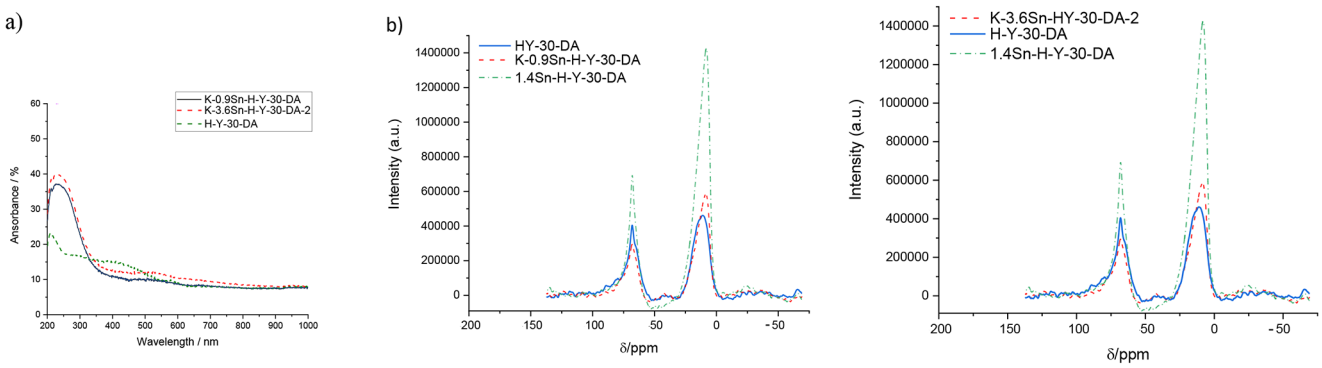

Fig. 8 **a**) UV-vis and **b**) solid state NMR-spectroscopy results of some selected catalysts

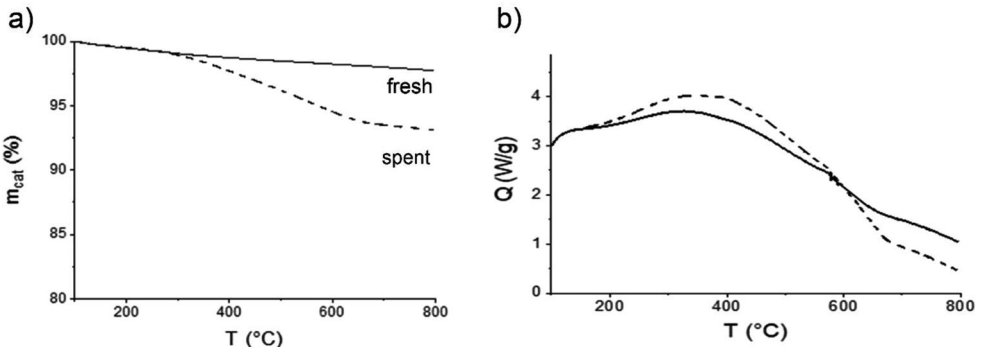

Fig. 9 The results from TGA analysis of K-0.9Sn-H-Y-30-DA, **a**) mass decrease, **b**) heat release as a function of temperature

Table 4 The results from CHNS analysis for some spent catalysts

Catalyst	Carbon (wt%/w)	Hydrogen (wt%/w)	Nitrogen (wt%/w)	Sulfur (wt%/w)	H/C ratio (wt%/w)
K-0.9Sn-H-Y-30-DA	2.9	0.63	0	0	2.6

high amount of silanol groups, which were not neutralized by potassium as was the case in [39]. As a conclusion it can be stated that both solid state NMR and UV-vis spectroscopy confirmed successful dealumination of the H-Y zeolite and removal of most of aluminium from the extra-framework structure.

No detectable basicity was observed for K-0.9Sn-H-Y-30-DA in temperature programmed desorption (TPD) of CO_2 and the peak eluting from the instrument exhibited the mass of 18 related to water (Fig. S3).

Analysis of Carbon Deposits

The amount of carbon deposits on the spent catalyst was quantified to be 4.6 wt% by TGA for K-0.9Sn-H-Y-30-DA, when the weight decrease of the spent catalyst was compared with that of the fresh catalyst (Fig. 9).

The CHNS analysis revealed that the coke generated on K-0.9Sn-H-Y-30-DA catalyst exhibited a hydrogen-to-carbon (H/C) molar ratio of 2.6 (Table 4). Comparison of this finding with the existing literature established that coke is predominantly comprised alkanes, consistent with an H/C ratio exceeding 2 [40].

The presence of coke or other deposits can lead to changes in accessibility and availability of different pore sizes, resulting in a modified pore size distribution [41].

Catalytic Results

Preliminary Results

A blank experiment was performed in the absence of any catalyst using glucose with the initial concentration of 0.05 mol/l in methanol at 180 °C and 30 bar total pressure for 24 h. A nearly complete conversion of glucose was obtained within 6 h giving 10% methyl lactate yield after 24 h (Fig. 10). This result is comparative with the literature data [20] reporting that glucose transformation was performed at 160ºC 4% methyl lactate was achieved after 10 h [20]. The initial glucose transformation rate in the absence of catalyst was 0.08 mmol/min in the current work. Rapid isomerization of glucose to fructose already took place in the first minutes and the initial formation rate of mannose was 0.02 mmol/min while for fructose it was only 0.002 mmol/min. After 24 h the carbon balance was only 7% and the reaction mixture contained also fructose, mannose and methyl levulinate with the yields of 2%, 2%, and 1%,

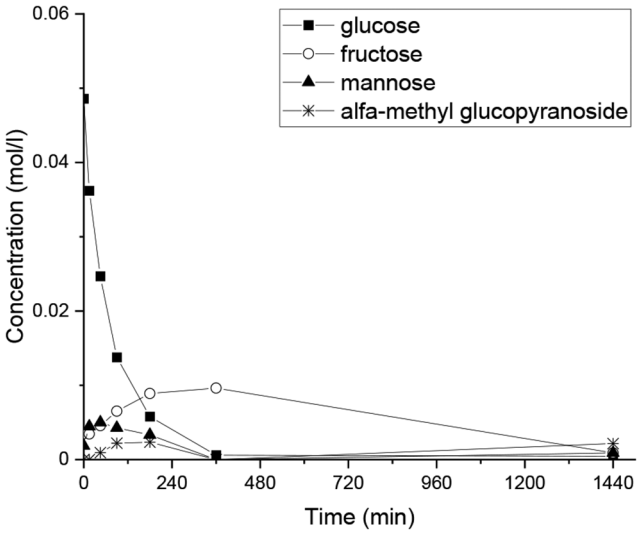

Fig. 10 Glucose transformation in methanol in the absence of any catalyst at 180°C and the initial glucose concentration of 0.05 mol/l

respectively. Most probably gaseous products as well as non-detectable humins and oligomers were formed.

Preliminary experiments over mesoporous, 1.4Sn-H-Y-30-DA and K-0.9Sn-H-Y-30-DA were performed at 180°C using 0.05 mol/l glucose in methanol (Table 5). The results showed that 96% conversion of glucose was reached already during heating over K-0.9Sn-H-Y-30-DA and 1.4Sn-H-Y-30-DA. The fructose concentration decreased after zero minute when stirring was started for 1.4Sn-H-Y-30-DA and for K-0.9Sn-H-Y-30-DA indicating that a lot of fructose was already formed during heating (Fig. 11a).

Etherification of glucose forming a-methylglucopyranoside was observed with K-0.9Sn-H-Y-30-DA which exhibited both weak and medium Brønsted acid sites (Table 3). It is known that glycosidation is promoted by the presence of Brønsted acid sites [41]. The dealuminated 1.4Sn-H-Y-30-DA catalyst exhibited a much higher amount of octahedrally and tetrahedrally coordinated Al than its K-containing counterpart according to ^{27}Al NMR-spectroscopy (Fig. 8b). Thus this result indicates that a certain amount of Brønsted acid sites facilitates reversible etherification and de-etherification.

Formation of methyl lactate and methyl levulinate analyzed by GC is also shown in Table 5. The results revealed superiority of K-0.9Sn-H-Y-30-DA giving 69% yield of methyl lactate at 180 °C confirming that the combination of K and Sn is beneficial for methyl lactate formation. Without K a large amount of methyl levulinate was formed over 1.4Sn-H-Y-30-DA due to its high acidity (Fig. 8b) and the methyl lactate yield was 30%. Carbon balance with this catalyst was also rather low (Table 5). Analogously it was reported in [42] that high BA/LA molar ratio promoted formation of methyl levulinate in glucose transformation at 170°C, especially over Sn-Al-USY catalyst, while alkali metal modification decreased this ratio and also formation of methyl levulinate. Furthermore, Sn supported on dealuminated Beta zeolite with BA/LA ratio of 0.02 gave 43.5% methyl lactate at 180°C [18]. It was decided that due to the low carbon balance the further experiments will be carried out at 150°C. Some additional experiments using different SiO_2/Al_2O_3 ratio were also performed. As a comparison the performance of Sn-modified Sn-H-Y-5.1 and Sn-H-Y-80 catalysts was studied at 150°C in glucose transformations. The yields of methyl lactate were after 24 h 1% and 11% for Sn-H-Y-5.1 and Sn-H-Y-80, respectively. The corresponding BA/LA ratios were for Sn-H-Y-5.1 and Sn-H-Y-80 4.5 and 0.7, respectively. These results demonstrated that a relatively low BA/LA ratio is beneficial for the methyl lactate production. However, when performance

Table 5 Yields of fructose (FRU), mannose (MAN), methyl lactate (MeLa), methyl levulinate (MeLe) and a-glucopyranoside (a-GLUPYR) at 180°C over different catalysts at complete conversion of glucose

Catalyst	$Y_{a-GLUPYR}$ (%)	Y_{FRU} (%)	Y_{MAN} (%)	Y_{MeLa} (%)	Y_{MeLe} (%)	Y_{MVG} (%)	CB (%)	Y_{total} (%)
1.4Sn-H-Y-30-DA (7)	3	0	0	30	24	6	58	64
K-0.9Sn-H-Y-30-DA (6)	0	0	0	69	1	12	78	82

[a] not detected

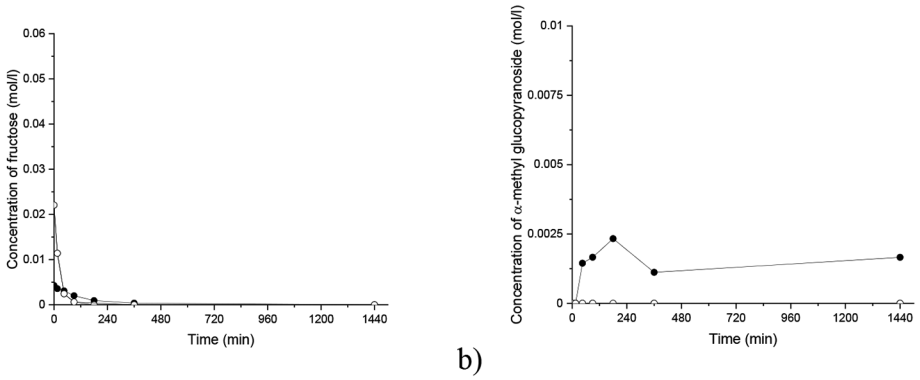

Fig. 11 Effect of different Sn and/or K-modified H-Y-catalysts on glucose transformations at 180°C with 0.41 g catalyst and the initial glucose concentration of 0.05 mol/l, (**a**) glucose, (**b**) fructose and (**c**) a-methylglucopyranoside as a function of time. Notation: 1.4Sn-H-Y-30-DA (**o**), K-0.9Sn-H-Y-30-DA (●)

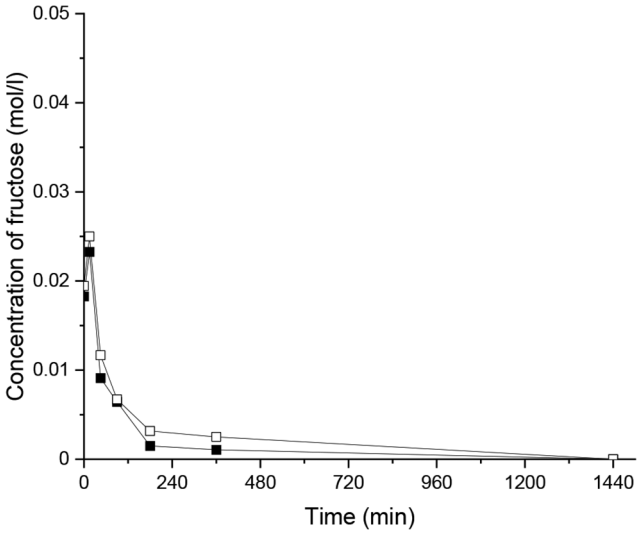

Fig. 12 Fructose concentration as a function of time in two repeated experiments over K-0.9Sn-H-Y-30-DA in glucose transformations at 150°C. Notation: experiment I (o), experiment II (■)

of K-Sn-H-Y-30-DA was compared with that of K-Sn-H-Y-80-DA, a higher methyl lactate yield was obtained with the former one, 72%, while over the latter one the corresponding yield was only 44%. These results show clearly that an optimum catalyst acidity is needed to promote formation of methyl lactate with too low acidity not being appropriate.

Repeatability of the experiments was evaluated using K-Sn-H-Y-30-DA-3 as a catalyst at 150°C under 30 bar in glucose transformations. Fructose concentrations in two experiments as a function of time (Fig. 12) show clearly that the difference in these concentrations is very small. In addition, differences in methyl lactate, methyl levulinate concentrations were below 5% after 24 h confirming good reproducibility of the experiments.

Effect of Microporous Sn-H-Y-30 on Glucose Transformation

Microporous Sn-H-Y-30 catalyst was investigated in glucose transformation at 150°C (Fig. 13b; Table 6). This catalyst exhibited a very high BA/LA ratio and a large Sn particle size (Tables 1 and 5). Large amounts of mannose and a-methylglucoside were formed over this catalyst and very high concentrations were still notable after 24 h with from $SnCl_2$ catalysts, which exhibited a low BA/LA ratio of 4.5. The results from GC analysis of the products after complete sugar transformation at 24 h are also shown in Table 6. It can be seen that the microporous Sn-modified H-Y-30 catalyst was not efficient in formation of methyl lactate. Carbon balance and the total yield were for this catalyst 80% and 83%, respectively. Large amount of undesired mannose was also formed over 22Sn-H-Y-30-EIM (Table 6, entry 1). Glucose epimerization to mannose could

Table 6 The yields of products for different Sn-H-Y catalysts prepared by the evaporation impregnation method. Conditions: 0.05 mol/l initial glucose concentration, 150°C, 30 bar, no sampling from the reactor. The results are given at complete glucose conversion. Notation: Glu glucose, Fru fructose, HMF 5-hydroxymethylfurfural, MMF methoxy methylfurfural, Fu furfural, methyl formate MeFo. Methyl formate and the products in "other identified products" column were not taken into carbon balance. The catalyst mass is 0.75 g if not otherwise stated

Entry	Catalyst	a-methyl glucoside (%)	Isomerisation products		Retro aldol cleavage		Fructose dehydration products			CB (%)	Y_{total} (%)
					[3+3]	[2+4]					
			Fructose (%)	D-Mannose (%)	Me-lactate (%)	Methyl vinyl glycolate (%)	Me-levulinate (%)	Methyl formate (%)	Other identified products (%)		
1	22Sn-H-Y-30-EIM	26	0	15	1	<1	36	5	0	73	78
2	K-0.9Sn-H-Y-30-DA	0	0	0	37	7	3	14	HMF<1	46	47
3	K-1.3Sn-H-Y-30-DA-4	0	0	0	55	8	4	8	0	56	67
4	K-1.4Sn-H-Y-30-DA-3	0	0	0	33	5	22	9	0	61	66
5	K-3.6Sn-H-Y-30-DA-2	1	0	0	53	8	6	15	0	68	69
6	K-H-Y-30-DA	5	19	0	6	0	2	9	MMF, Tra58ces Glu 2	34	34
7	Sr-2.5Sn-H-Y-30-DA	0	0	0	48	8	0	0	HMF 1; MMF 2; Fu 1	55	58
8	Cs-0.6Sn-H-Y-30-DA	0	0	0	42	7	5	8	MMF 3	53	54
9	K-1.3Sn-H-Y-30-DA-4, m_{cat}=0.45 g	0	0	0	72	11	1	7	0	85	87
10	K-1.3Sn-H-Y-30-DA-4 m_{cat}=0.60 g	0	0	0	53	7	2	7	0	65	65
11	K-1.3Sn-H-Y-30-DA-4, m_{cat}=0.90 g	0	0	0	65	10	4	10	0	74	77
12	K-1.3Sn-H-Y-30-DA-4, m_{cat}=1.05 g	0	0	0	65	13	1	13	0	74	78

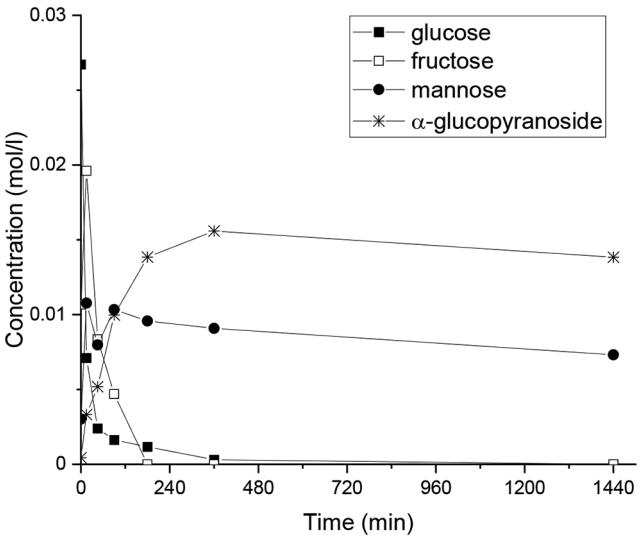

Fig. 13 Concentrations of glucose, fructose, mannose and a-methyl-glucopyranoside over 22Sn-H-Y-30-EIM in glucose transformation at 150°C. Initial glucose concentration is 0.07 mol/l

be hindered by replacement of adjacent to Sn acidic silanol (Si-OH) groups with potassium in the zeolite [43]. Fructose can undergo also epimerization to mannose or alternatively retro-aldol cleavage in the presence of Lewis acid sites [44]. In [45] it was reported that mannose selectivity remained constant in glucose transformation over K-Sn-MCM-41, while selectivity to fructose decreased indicating that mannose was formed from glucose.

Effect of Alkali Metal Modification of Mesoporous Sn-H-Y-30 Catalysts on Glucose Transformation

The performance of H-Y-30-DA was investigated in glucose transformation using both K-Sn (Table 6, entry 2) as well as only potassium modified catalysts (Table 6, entry 6).The results showed that methyl lactate was 70%, when the catalyst contains both K- and Sn.

The effect of different alkali metals on the performance of Sn-H-Y-30-DA-2 is demonstrated in Fig. 14; Table 6. Glucose was already converted during heating as follows: 97%, 100% and 71% over K-, Cs- and Sr-2.5Sn-H-Y-30-DA-2, respectively. Analogous results with high glucose transformation rates over Sn-H-Beta zeolite have been reported in [12]. The experiments were conducted at 150oC, as higher temperatures would lead to a decline in selectivity related to well-known excessive formation of humins.

Much slower rates for fructose disappearance were observed for K- and Sr-modified Sn-H-Y-30-DA-2 catalyst in comparison to Cs-Sn-H-Y-30. Although high concentration of Lewis acid sites in Sr-modified catalyst promoted fructose reaction further in [45], K-3.6Sn-H-Y-30-DA-2 contained also high amount of Brønsted acid sites with medium strength (Table 3) and thus promoted etherification of glucose. At the same time fructose formation and its further transformation was retarded. Noteworthy is also that Sr-2.5Sn-H-Y-30-DA-2 has also medium and strong Brønsted acid sites not present in two other materials and it catalyzed also reversible etherification. Glucose epimerization to undesired mannose was also more prominent over Sr-modified Sn-H-Y-30-DA, which exhibited also strong Brønsted acid sites.

The GC analysis after 24 h revealed that the best catalyst in Sr-, Cs- and K- modified Sn-H-Y-30-DA-2 catalyst series gave the following methyl lactate yields: 48%, 42% and 37%, respectively (Table 6, entries 2, 7 and 8). It should also be pointed out that all of these catalysts exhibited 6–7.4 nm metal particle sizes (Table S1). Noteworthy is also that methyl levulinate yield over these catalysts was very small while the carbon balances (entries 2, 7, 8) were below 55%. In addition to products, which were quantified, also some C3 ethers and other products were identified in GC-MS analysis (Fig. S4). As a comparison Sr-modified microporous Sn-Al-Beta catalyst giving a higher yield of methyl lactate, 53%, exhibited a higher acid site concentration and a higher BA/LA ratio (0.8) [13] than in the current case for Sr-Sn-H-Y-DA-30-2. One reason might be the higher availability of the acid sites in the latter case.

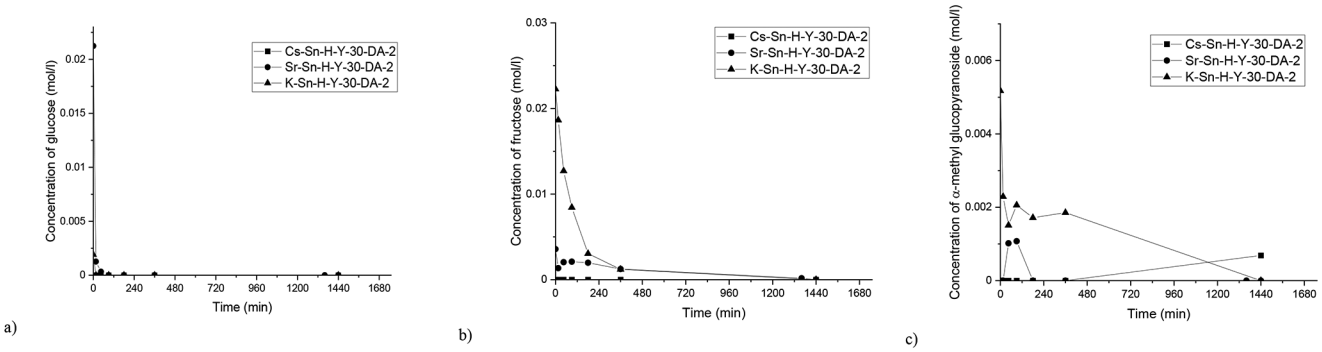

Fig. 14 Concentration of (**a**) glucose, (**b**) fructose, (**c**) a-methyl glucopyranoside over different alkali modified H-Y-30-DA catalysts. Initial glucose concentration is 0.07 mol/l

The highest methyl levulinate yield was obtained with K-1.4Sn-H-Y-30-DA-3 (Table 6, entry 4), which contained the highest amount of Brønsted acid sites with medium strength (Table 3). As a comparison with literature [44] methyl levulinate yield increased with increasing Sn loading over dealuminated Sn-H-Beta catalysts in glucose transformation in water at 110°C. In [44] it was stated that higher loadings of Sn increased the amounts of less active condensed SnO_x species, when Sn dispersion decreased.

The yield of methyl lactate was not affected much on Sn particle size when comparing methyl lactate yields (Table 6, entries 2–5) with Sn particle sizes (Table S1). However, with a very high tin loading, such as in 22Sn-HY-30-EIM with large Sn particle size of 11 nm (Table S1), only 1% of methyl lactate was obtained. Mesoporous dealuminated catalysts exhibited also low BA/LA ratio giving high yields of methyl lactate, while high BA/LA yields and mesoporosity, also previously reported, was desirable for methyl levulinate formation. The highest methyl lactate yield was obtained over K-1.3Sn-H-Y-30-DA-4, 55% (Table 6, entry 3). Although majority of SnO_2 in the current work is located outside of the framework, it cannot be excluded that some SnO_2 particles are also inside the cavities. Due to a larger size of glucose, 0.86 nm [45] in comparison to the pore size of faujasite, being 0.74 nm [37], some large organic molecules can suffer from diffusional limitations [40] and thus activity and selectivity can be decreased when using microporous catalysts.

As a comparison with the literature, one of the highest yields of methyl lactate, 69% at 160°C was achieved over mesoporous Sn-In-MCM-41 [19]. In addition, for K-Sn-USY ca. 70% methyl lactate yield at 150°C was reported [17]. Furthermore, ca. 52% methyl lactate yield was obtained over hierarchical Sn-Beta zeolite at 160°C under 5 bar in 6 h [14]. XRD results of this catalyst showed no presence of SnO_2 peaks indicating high dispersion of Sn species [14]. Analogously no SnO_2 peaks were visible in XRD pattern for K-Sn-USY, which was an efficient catalyst for methyl lactate production [17].

For the best performing K-1.3Sn-H-Y-30-DA-4 catalyst (Table 6, entry 3) different catalyst amounts were also tested (Table 6, entries 3, 9–12). The results showed that an optimum amount of catalyst, 0.45 g gave 72% yield of methyl lactate and high carbon balance, 85%. However, at the same time, relatively high amount of methyl vinyl glycolate was also formed. When calculating the ratio of the yield of MVG to yield of MeLa it remained in the range of 0.09–0.17, while high Y_{MVG}/Y_{MeLa} ratio was obtained over 22Sn-H-Y-30-EIM, with the highest mass of K1.3Sn-H-Y-30-DA-4, and with K0.9Sn-H-Y-30-HA, which contained only a small amount of Sn. These results showed that methyl lactate and methyl vinylglycolate are formed parallelly over Sn-modified catalysts. This result is in accordance with those of [42]. In their case [42] Sn-Al-USY catalyst with BA/LA ratio of 0.151 produced after 6 h ca. 10% methyl lactate and 2% methyl vinyl glycolate, while its potassium exchanged counterpart with BA/LA ratio of 0.034 gave 42% methyl lactate and 10% methyl vinyl glycolate in glucose transformation at 170°C.

An attempt was made to rationalize the catalytic data and correlate it with the catalyst properties via plotting the carbon balance, yield of methyl lactate, methyl vinyl glycolate and methyl levulinate as a function of the molar ratio of Brønsted acid sites to glucose and Lewis acid sites to glucose (Fig. 15). The carbon balance was very low for K-H-Y-30-DA and for K-0.9Sn-H-Y-30-DA. The former catalyst exhibited no Brønsted acidity while that latter one has the highest Brønsted to Lewis acid site ratio (Table 3). The reason for a low carbon balance over mild acidic catalysts is that organic molecules adsorb strongly on the catalyst surface, although the rate for the product formation is low. On the other hand, high acidity of the catalyst results in a low carbon balance and formation of large amounts of unknown products as reported also in [16] over Sn-USY catalyst with a high amount of strong Brønsted acid sites. On the other hand, with a low amount of K-1.3Sn-H-Y-30-DA-4 and a low molar ratio of BA/glucose the highest carbon balance was obtained.

It can be clearly seen from Table 6; Fig. 15 that the mesoporous catalyst K-H-Y-30-DA without Sn gave low yield of both methyl lactate, vinyl glycolate and levulinate and it is noteworthy that 19% of unconverted fructose was present in the reaction mixture after 1440 min. Although this catalyst has high Lewis acidity, but no Brønsted acidity low yield of methyl lactate was obtained. This result showed that both Brønsted and Lewis acid sites are required. However, already a small amount of Lewis and Brønsted acid sites promoted methyl lactate formation giving 72% yield after 1440 min with K-1.3Sn-H-Y-30-DA-4 exhibiting both weak Brønsted and Lewis acid sites. This result is in accordance with those reported in [46] in which sucrose was transformed to methyl lactate over Mg-modified Sn Beta. When in the current work the catalyst was dealuminated only once, i.e. K-0.9Sn—H-Y-30-DA exhibited too high amount of Brønsted acid sites (Table 3) and was not efficient for production of methyl lactate. The dealuminated catalyst with a high tin loading, K-3.6Sn-H-Y-30-DA-2 gave the second highest methyl lactate yield, however, also more levulinic acid than obtained over K-1.3Sn-H-Y-30-DA-4. These results show that multiple dealumination steps and small amount of catalyst were required to synthesize a good catalyst for methyl lactate production. As a comparison, the microporous 22Sn-H-Y-30-EIM gave mainly methyl levulinate due to its high Brønsted acidity. The formation of methyl vinyl glycolate

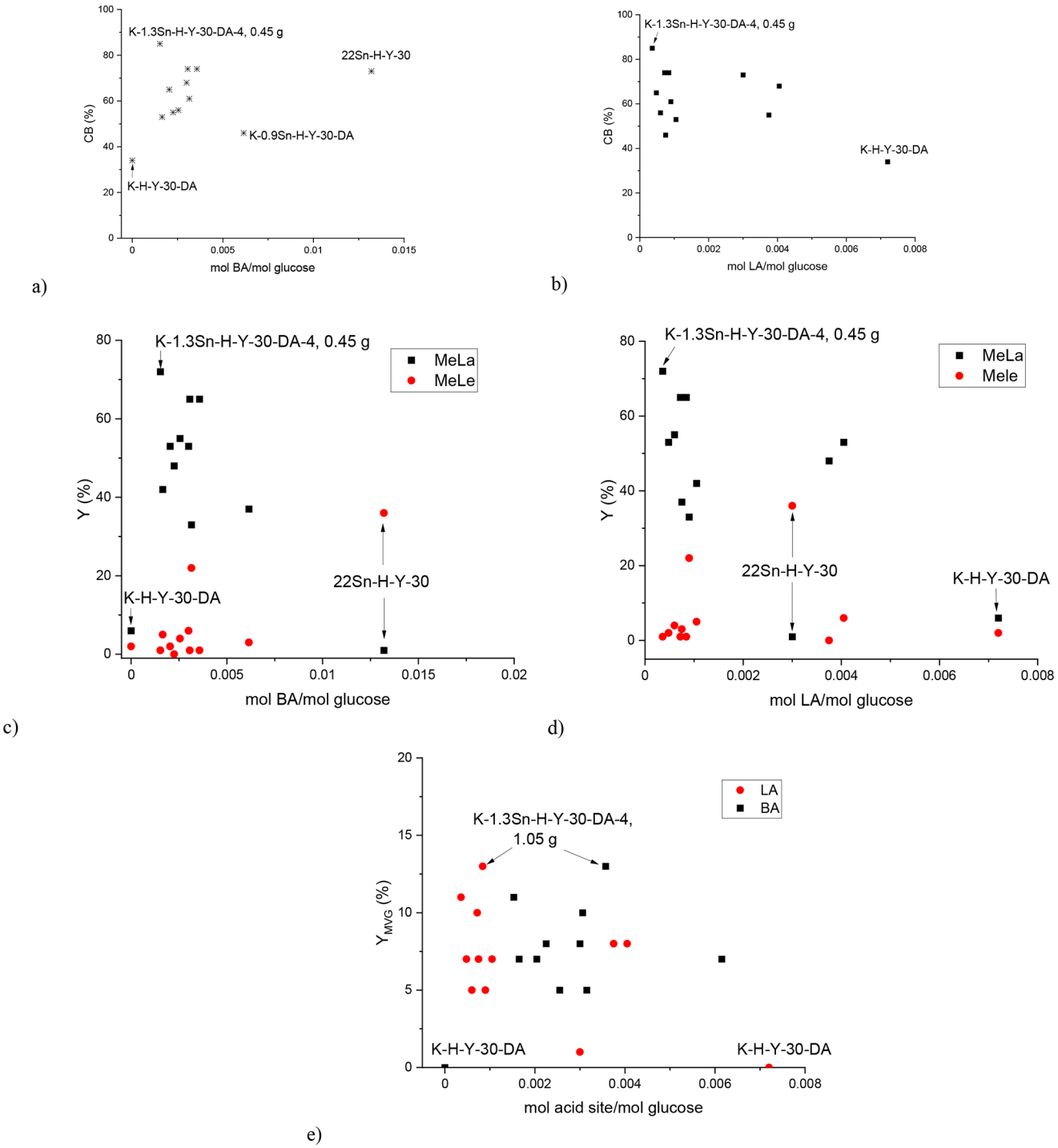

Fig. 15 (**a**) The carbon balance as a function of the molar ratio of Brønsted acid sites to glucose, (**b**) the carbon balance as a function of the molar ratio of Lewis acid sites to glucose, (**c**) yield of methyl lactate (MeLa) and methyl levulinate (MeLe) as a function of the molar ratio of BA to glucose, **e**) yield of methyl vinyl glycolate as a function of molar ratio of Brønsted acid to glucose and Lewis acid to glucose calculated and (**d**) molar ratio of Lewis acid sites (LA) to glucose. Data is taken from Table 6. Conditions: glucose transformation after 1440 at 150°C

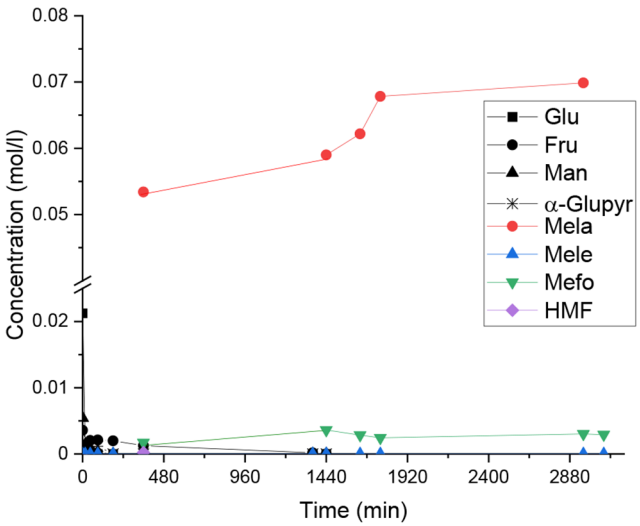

Fig. 16 Concentrations of glucose and products in glucose transformation over Sr-2.5Sn-H-Y-30-DA-2 at 150 °C, 30 bar (up to 1440 min) and without the catalyst after filtering it away

was high with a high amount of K-1.3Sn-H-Y-30-DA-4, while no methyl vinyl glycolate was formed over K-H-Y-30-DA in the absence of tin.

Filtration Test

The filtration test was performed for the reaction with Sr-2.5Sn-H-Y-30-DA-2 as a catalyst. The results confirmed that the reaction proceeded after filtering away the solid catalyst after 1440 min and continuing the experiment with the filtrate (Fig. 16), indicating also presence of homogeneous catalysis, i.e. by leached metals. Sn amount decreased by ca. 14% when applying Sn-Beta catalyst in continuous glucose transformation in methanol. In addition, in water the metal leaching was 19% [45]. An opposite result was obtained in glucose transformations over hierarchical Sn-Beta catalyst [14].

Catalyst Regeneration and Reuse

Catalyst regeneration and the reuse test was performed over K-1.3Sn-H-Y-30-DA-4, which exhibited the best performance maximizing the yield of methyl lactate (Table 6, entry 3). The results showed that complete glucose conversion was achieved within just 30 min, the methyl lactate yield was only 33% while methyl levulinate yield increased from 4 to 21% when the regenerated catalyst was reused. In addition to methyl levulinate also the yield of methyl vinyl glycolate was increased over the regenerated catalyst, which is an interesting observation requiring a separate investigation. It should, however, be pointed out here that the calcination temperature, 400°C, might be too low, as for example, a higher calcination temperature of 550°C was used in [17]. Moreover, the metal leaching has occurred [47] as described in Sect. 3.1.4. Obviously further efforts are needed to improve the catalyst stability.

Conclusions

The performance of a microporous Sn-modified H-Y-30 (number denotes SiO_2/Al_2O_3 ratio) catalyst prepared by the evaporation impregnation methods as well as mesoporous Sn- and/or alkali metal modified H-Y zeolites prepared by ion exchange were characterized and tested in glucose transformations to methyl lactate in a batch reactor. The dealuminated K-Sn-H-Y-30 catalysts did not contain strong Brønsted acid sites, while Sr-Sn-H-Y-30-DA exhibited small amounts of strong acid sites. ^{27}Al MAS NMR-spectroscopy results showed that modification of Sn-H-Y-30-DA with potassium decreased both Lewis and Brønsted acid site concentration. The presence of isolated Sn^{IV} species was confirmed in Sn-H-Y-30-DA catalysts.

For microporous Sn-modified H-Y-30 maximally 1% yield of methyl lactate was obtained. Furthermore, large amounts of methyl levulinate were formed over this catalyst. The low yield of methyl lactate can be explained by large amounts of medium and strong acid sites over this catalyst.

For mesoporous, dealuminated K- and Sn-modified H-Y-30 the highest amount of methyl lactate, 72% was obtained in glucose transformation at 150°C. This catalyst exhibited Sn particle size of 5.3 nm and loading of 1.3 wt%. The Brønsted to Lewis acid ratio of this catalyst devoid from medium and strong Brønsted acid site and it was 4.3. In addition, the carbon balance with this catalyst in the liquid phase was 56%. It was also observed that with increasing Sn-loadings the yield of methyl lactate decreased. Sr- and Cs-modified Sn-H-Y-30-DA catalysts gave only 42% and 48% yield of methyl lactate, respectively. A hot filtration test of Sr-Sn-H-Y-30-DA demonstrated that the homogeneous reaction took place after filtration of the catalyst. Metal leaching was also confirmed for K-Sn-H-Y-30-DA showing that more efforts should be put to stabilise K and Sn or embed them into the support.

Supplementary Information The online version contains supplementary material available at https://doi.org/10.1007/s12649-0

25-02930-z.

Author Contribution All authors contributed to the study conception and design. Material preparation, data collection and analysis were performed by Ramin Majidov, Atte Aho, Zuzana Vajglova, Robert Lassfolk, Ilari Angervo and Mika Lastusaari. The first draft of the manuscript was written by Ramin Majidov and Päivi Mäki-Arvela and all authors commented on previous versions of the manuscript. All authors read and approved the final manuscript.

Funding Open access funding provided by Åbo Akademi University. Samples for electron microscopy were processed and analyzed at the Electron Microscopy Laboratory, Institute of Biomedicine, University of Turku, which receives financial support from Biocenter Finland.

Data Availability The datasets generated during and/or analysed during the current study are available from the corresponding author on reasonable request.

Declarations

Competing Interests The authors have no relevant financial or non-financial interests to disclose.

References

1. Świątek, K., Gaag, S., Klier, A., Kruse, A., Sauer, J., Steinbach, D.: Acid hydrolysis of lignocellulosic biomass: Sugars and furfurals formation. Catalysts. **10**, 437 (2020)
2. Vajglová, Z., Yevdokimova, O., Medina, A., Eränen, K., Tirri, T., Hemming, J., Lindén, J., Angervo, I., Damlin, P., Doronkin, D.E., Mäki-Arvela, P., Murzin, D.: Solventless hydrodeoxygenation of isoeugenol and dihydroeugenol in batch and continuous modes over a zeolite-supported FeNi catalyst. Sustainable Energy Fuels. **7**, 4486–4504 (2023)
3. Mäki-Arvela, P., Salmi, T., Holmbom, B., Willför, S., Murzin, D.Y.: Synthesis of sugars by hydrolysis of hemicelluloses- a review. Chem. Rev. **111**, 5638–5666 (2011)
4. Mäki-Arvela, P., Aho, A., Murzin, D.Y.: Heterogeneous catalytic synthesis of methyl lactate and lactic acid from sugars and their derivatives. ChemSusChem. **13**, 4833–4855 (2020)
5. Aho, A., Kumar, N., Eränen, K., Mäki-Arvela, P., Salmi, T., Peurla, M., Angervo, I., Hietala, J., Murzin, D.Y.: Catalytic conversion of glucose to methyl levulinate over metal-modified Beta zeolites. Reac Kinet Mech. Cat. **135**, 1971–1986 (2022)
6. Abdel-Rahman, M.A., Tashiro, Y., Sonomoto, K.: Recent advances in lactic acid production by microbial fermentation processes. Biotechnol. Adv. **31**, 877–902 (2013)
7. Rawoof, S.A.A., Kumar, P.S., Vo, D.-V.N., Devaraj, K., Mani, Y., Devaraj, T., Mani, Y., Devaraj, T.: Production of optically pure lactic acid by microbial fermentation: A review. Environ. Chem. Lett. **9**, 539–556 (2021)
8. Zhang, L., Theng, D.S., Du, Y., Xi, S., Huang, L., Gao, F., Wanh, L., Chen, A., Borgna, A.: Selective conversion of lactic acid to acrylic acid over alkali and alkaline-earth metal co-modified NaY zeolites. Catal. Sci. Technol. **7**, 6101–6111 (2017)
9. de Oliveira, R.A., Komesu, A., Rossell, V., Maciel, C.E.: Challenges and opportunities in lactic acid bioprocess design—from economic to production aspects. Biochem. Eng. J. **133**, 219–239 (2018)
10. Yang, X., Wang, Y., Su, Y., Zhou, L.: Influence of sn content in Sn-β on selective production of methyl lactate from glucose. Catal. Lett. **2153**, 1773–1785 (2023)
11. Tosi, I., Riisager, A., Taarning, E., Jensen, P., Meier, S.: Kinetic analysis of hexose conversion to methyl lactate by Sn-Beta: Effects of substrate masking and of water. Catal. Sci. Techn. **8**, 2137–2145 (2018)
12. Aho, A., Kumar, N., Eränen, K., Lassfolk, R., Mäki-Arvela, P., Salmi, T., Peurla, M., Angervo, I., Hietala, J., Murzin, D.Y.: Improving the methyl lactate yield from glucose over Sn–Al-Beta zeolite by catalyst promoters. Microp Mesop. Mat. **351**, 112483 (2023)
13. Tang, B., Li, S., Song, W.-C., Yang, E.-C., Zhao, X.-J., Guan, N., Li, L.: Fabrication of hierarchical Sn-beta zeolite as efficient catalyst for conversion of cellulosic sugar to methyl lactate. ACS Sustainable Chem. Eng. **8**, 3796–3808 (2020)
14. Yang, X., Wang, L., Lu, T., Gao, B., Su, Y., Zhou, L.: Seed-assisted hydrothermal synthesis of Sn-Beta for conversion of glucose to methyl lactate: Effects of the H2O amount in the gel and crystallization time. Catal. Sci. Technol. **10**, 8437–8444 (2020)
15. Qu, H., Zhou, S., Su, Y., Yang, X., Zhou, L.: Cost-effective and fast synthesis of Sn-β zeolite with less silanol defects for efficient conversion of glucose to methyl lactate. Mol. Catal. **524**, 112259 (2022)
16. Jimenez-Martin, J.M., Orozco-Saumell, A., Hernando, H., Linares, M., Mariscal, R., López Granados, M., Garcia, A., Iglesias, J.: Efficient conversion of glucose to methyl lactate with Sn-USY: Retro-aldol activity promotion by controlled ion exchange. ACS Sustainable Chem. Eng. **10**, 8885–8896 (2022)
17. Yue, X.-Y., Ren, H.-F., Wu, C., Xu, J., Li, J., Liu, C.-L., Dong, W.-S.: Highly efficient conversion of glucose to methyl lactate over hierarchical bimetal-doped Beta zeolite catalysts. J. Chem. Techn Biotechn. **96**, 2238–2248 (2021)
18. de la Iglesia, Ó., Sarango, M., Munárriz, M., Malankowska, M., Navajas, A., Gandía, L.M., Coronas, J., Téllez, C.: Mesoporous Sn-In-MCM-41 catalysts for the selective sugar conversion to methyl lactate and comparative life cycle assessment with the biochemical process. ACS Sustainable Chem. Eng. **10**, 868–2880 (2022)
19. Yang, X., Liu, Y., Li, X., Ren, J., Zhou, L., Lu, T., Su, Y.: Synthesis of Sn-containing nanosized beta zeolite as efficient catalyst for transformation of glucose to methyl lactate. ACS Sustainable Chem. Eng. **26**, 8256–8265 (2018)
20. Navar, R., Botti, L., Tarantino, G., Hammond, C.: Catalytic performances of Sn-Beta catalysts prepared from different heteroatom-containing beta zeolites for the retro-aldol fragmentation of glucose. Reactions. **3**, 265–282 (2022)
21. Bayu, A., Karnjanakom, S., Yoshida, A., Kusakabe, K., Abudula, A., Guan, G.: Polyoxomolybdates catalysed cascade conversions of cellulose to glycolic acid with molecular oxygen via selective aldohexoses pathways (an epimerization and a [2+4] retro-aldol reaction). Catal. Today. **332**, 28–34 (2019)

22. Majidov, R.: Sustainable feedstock to acrylic acid using H-Y zeolites, Master thesis, Åbo Akademi University, (2023). https://www.doria.fi/handle/10024/187633
23. Pethő, D., Kurusta, T., Kristály, F., Mikó, T., Gácsi, Z.: The effect of ball to powder ratio on the processing of a novel Mo-Cu-Al_2O_3 composite. Int. J. Refract. Met. Hard Mater. **101**, 105657 (2021)
24. Emeis, C.A.: Determination of integrated molar extinction coefficients for infrared absorption bands of pyridine adsorbed on solid acid catalysts. J. Catal. **141**, 347–354 (1993)
25. Jeanjean, J., Aouali, L., Delafosse, D., Dereigne, A.: Crystal structure of different dealuminated Y-type zeolites determination of framework vacancies and non-framework species. J. Chem. Soc. Faraday Trans. **1 85**, 2771–2783 (1989)
26. Baur, W.H., Khan, A.A.: Rutile-type compounds. IV. SiO2, GeO2 and a comparison with other rutile-type structures. Acta Crystallogr. Sect. B. **27**, 2133–2139 (1971)
27. Chu, Y., Chen, S., Zheng, J., Li, Z.: Elimination of oxidation and decomposition by $SnCl_2$ in the SERS study of pyridoxine on a roughened au electrode. J. Raman Spectrosc. **40**, 229–233 (2009)
28. Wei, B., Jin, L., Wang, D., Xiong, Y., Hu, H., Bai, Z.: Effect of different acid-leached USY zeolites on *in-situ* catalytic upgrading of lignite tar. Fuel. **266**, 117089 (2020)
29. Remy, M.J., Stanica, D., Poncelet, G., Feijen, E.J.P., Grobet, P.J., Martens, J.A., Jacobs, P.A.: Dealuminated H–Y zeolites: Relation between physicochemical properties and catalytic activity in heptane and decane isomerization. J. Phys. Chem. **100**, 12440–12447 (1996)
30. Zhang, L., Chen, K., Chen, B., White, J.L., Resasco, D.E.: Factors that determine zeolite stability in hot liquid water. J. Am. Chem. Soc. **137**, 11810–11819 (2015)
31. Wang, K., Yang, Z., Ma, Y., Zhao, W., Sun, J., Lu, T., He, H.: Recent advances in the utilization of glycerol for the production of lactic acid by catalysis. Biofuels, Bioprod. Biorefin. **16**, 1428–1454 (2022)
32. de Jong, K.P., Zečević, J., Friedrich, H., de Jongh, P.E., Bulut, M., van Donk, S., Kenmoge, R., Finiels, A., Hulea, V., Fajula, F.: Zeolite Y crystals with trimodal porosity as ideal hydrocracking catalysts. Ang Chem. Int. Ed. **49**, 10074–10078 (2010)
33. Harris, J.W., Cordon, M.J., Di Iorio, J.R., Vega-Vila, J.C., Ribeiro, F.H., Gounder, R.: Titration and quantification of open and closed Lewis acid sites in Sn-Beta zeolites that catalyze glucose isomerization. J. Catal. **335**, 141–154 (2016)
34. Paris, C., Moliner, M., Corma, A.: Metal-containing zeolites as efficient catalysts for the transformation of highly valuable chiral biomass-derived products. Green. Chem. **15**, 2101–2109 (2013)
35. Jin, J., Ye, X., Li, Y., Wang, Y., Li, L., Gu, J., Zhao, W., Shi, J.: Synthesis of mesoporous Beta and Sn-Beta zeolites and their catalytic performances. Dalton Trans. **43**, 8196–8204 (2014)
36. Bai, J., Ling, W., Chen, W., Liu, Y., Sun, P., Wang, H., Wang, C.: The role of aluminum in Sn-Al-beta zeolite catalyzing the conversion of glucose to methyl lactate. Mol. Catal. **541**, 113071 (2023)
37. Li, S., Zheng, A., Su, Y., Fang, H., Shen, W., Yu, Z., Chen, L., Deng, F.: Extra-framework aluminium species in hydrated faujasite zeolite as investigated by two-dimensional solid-state NMR spectroscopy and theoretical calculations. Phys. Chem. Chem. Phys. **12**, 3895–3903 (2010)
38. Deng, F., Yue, Y., Ye, C.: Observation of Nonframework Al species in zeolite β by solid-state NMR spectroscopy. J. Phys. Chem. B. **102**, 5252–5256 (1998)
39. Jiménez-Martin, J.M., El Tawil-Lucas, M., Montaña, M., Linares, M., Osatiashtiani, A., Vila, F., Alonso, D., Moreno, J., Garcia, A., Iglesias, J.: Production of methyl lactate with Sn-USY and Sn-β: Insights into real hemicellulose valorization. ACS Sustainable Chem. Eng. **12**, 2771–2782 (2024)
40. Cain, J., Laskin, A., Kholghy, M.R., Thomson, M.J., Wang, H.: Molecular characterization of organic content of soot along the centerline of a coflow diffusion flame. Phys. Chem. Chem. Phys. **16**, 25862–25875 (2014)
41. Saravanamurugan, S., Paniagua, M., Melero, J.A., Riisager, A.: Efficient isomerization of glucose to fructose over zeolites in consecutive reactions in alcohol and aqueous media. J. Am. Chem. Soc. **135**, 5246–5249 (2013)
42. Iglesias, J., Moreno, J., Morales, G., Melero, J.A., Juárez, P., López-Granados, M., Mariscal, R., Martinez-Salazar, I.: Sn–Al-USY for the valorization of glucose to methyl lactate: Switching from hydrolytic to retro-aldol activity by alkaline ion exchange. Green. Chem. **21**, 5876–5885 (2019)
43. Otomo, R., Kosugi, R., Kamiya, Y., Tatsumi, T., Yokoi, T.: Modification of Sn-Beta zeolite: Characterization of acidic/basic properties and catalytic performance in Baeyer–Villiger oxidation. Catal. Sci. Technol. **6**, 2787–2795 (2016)
44. Li, S., Josephson, T., Vlachos, D.G., Caratzoulas, S.: The origin of selectivity in the conversion of glucose to fructose and mannose in Sn-BEA and Na-exchanged Sn-BEA zeolites. J. Catal. **355**, 11–16 (2017)
45. Pimenta Lorenti, J., Scolari, E., Cabral, N.M., Bisio, C., Gallo, J.M.R.: Isomerization and epimerization of glucose catalyzed by Sn-containing mesoporous silica. Ind. Eng. Chem. Res. **60**, 12821–12833 (2021)
46. Yang, X., Hu, J., Lu, T., Zhou, L.: The important role of weak Brønsted acid site of Sn-β in conversion of sucrose to methyl lactate. Mol. Catal. **536**, 112908 (2023)
47. Zhang, Y., Luo, H., Zhao, X., Zhu, L., Miao, G., Wang, H., Kong, L.: Continuous conversion of glucose into methyl lactate over the Sn-Beta zeolite: Catalytic performance and activity insight. Ind. Eng. Chem. Res. **59**, 17365–17372 (2020)